Kinetic theory of simple granular shear flows of smooth hard spheres

By J. M. MONTANERO[1], V. GARZÓ[2],
A. SANTOS[2] and J. J. BREY[3]

[1] Departamento de Electrónica e Ingeniería Electromecánica, Universidad de Extremadura,
E-06071 Badajoz, Spain

[2] Departamento de Física, Universidad de Extremadura, E-06071 Badajoz, Spain

[3] Física Teórica, Universidad de Sevilla, E-41080 Sevilla, Spain

Steady simple shear flows of smooth inelastic spheres are studied by means of a model kinetic equation and also of a direct Monte Carlo simulation method. Both approaches are based on the Enskog equation and provide for each other a test of consistency. The dependence of the granular temperature and of the shear and normal stresses on both the solid fraction and the coefficient of restitution is analysed. Quite a good agreement is found between theory and simulations in all cases. Also, simplified expressions based on the analytical solution of the model for small dissipation are shown to describe fairly well the simulation results even for not small inelasticity. A critical comparison with previous theories is carried out.

1. Introduction

In rapid granular flows, particle interactions can be described as instantaneous collisions and the motion of individual grains is analogous to the thermal motion of molecules in a gas. However, collisions between granular particles are inelastic and frictional, so that the extension of the kinetic theory of molecular gases accounts for these dissipation mechanisms (Jenkins & Savage 1983; Lun *et al.* 1984; Jenkins & Richman 1985; Goldshtein & Shapiro 1995; Brey, Dufty & Santos 1997*a*). In the simplest versions, the grains are modelled as smooth, inelastic, hard spheres or disks. Inelasticity is characterized by means of a constant coefficient of normal restitution. In this way, generalizations of the Boltzmann and Enskog equations for inelastic particles have been derived. From these kinetic equations, exact macroscopic balance equations are easily obtained by taking appropriate velocity moments. Nevertheless, they only provide a true closed hydrodynamic description after explicit expressions for the pressure tensor, the heat flux and energy source term are obtained. This requires, in general, solving the kinetic equation under consideration.

Almost all analytical studies of the Boltzmann and Enskog equations have been restricted to near equilibrium situations, for which approximate solutions to the equations have been found. Very little is known about solutions describing far from equilibrium states. This is true for both molecular fluids and granular flows, but the difficulties are even harder for the latter, since dissipation in collisions is coupled to spatial inhomogeneities in a rather non-trivial way. For instance, it is easily seen that a granular system with uniform boundaries at constant temperature develops spatial inhomogeneities spontaneously (Brey & Cubero 1998).

One of the simplest non-equilibrium states one can think of is simple or uniform shear flow. Macroscopically, it is characterized by a constant linear velocity profile and uniform density and temperature. This state has been extensively studied for molecular as well as for granular systems. Nevertheless, the nature of the state is quite different in each system. While for elastic fluids the temperature increases monotonically in time due to viscous heating, a steady state is possible for granular media when the effect of the viscosity is exactly compensated by the dissipation in collisions. It is precisely this steady state that we are interested in here.

Although steady simple shear flow has been the subject of many previous works, most of them are based on a Navier–Stokes description of the hydrodynamic fields and, therefore, they are restricted to small velocity gradients, which for this state is equivalent to small inelasticity. This was the method used by Lun *et al.* (1984) to get the rheological properties as functions of the coefficient of restitution and the density. On the other hand, the only general theory for arbitrary shear rate we are aware of was formulated by Jenkins & Richman (1988). They used a maximum-entropy approximation in the Enskog equation to get a closed set of equations for the elements of the pressure tensor. The equations are too complicated to be solved in general, and additional approximations were introduced in order to analyse the limits of dilute and dense systems. The theory predicts anisotropy of the pressure tensor, i.e. normal stress differences, an effect that cannot be derived from the Navier–Stokes approximation. In this context, let us mention that Sela, Goldhirsch & Noskowicz (1996) have been able to obtain a perturbative solution of the Boltzmann equation up to Burnett order, i.e. transport equations to third order in the shear rate. At this order the normal stress differences show up.

The aim of this paper is to carry out a detailed study of the steady simple shear flow in the framework of the Enskog theory. Two complementary routes will be employed: a model kinetic equation and direct Monte Carlo simulations. Model kinetic equations that preserve the critical physical and mathematical properties of the original Enskog or Boltzmann equations are useful in order to allow a detailed analysis of granular flows. Here we will use a model for inelastic gases (Brey *et al.* 1997*a*) that has been introduced very recently as an approximation of the Enskog equation or, more precisely, of a modified version of it, the so-called revised Enskog theory (RET) (van Beijeren & Ernst 1973; Brey *et al.* 1997*a*). On the other hand, a very efficient numerical Monte Carlo simulation method has been proposed recently (Montanero & Santos 1996, 1997*a*). It is an extension to the RET of the direct simulation Monte Carlo method developed over the past twenty years for solving the Boltzmann equation for molecular fluids (Bird 1994). The method is equally suitable for both elastic and inelastic collisions. Comparison between the model kinetic predictions and the simulation results allows us to derive approximate expressions for the elements of the pressure tensor as explicit functions of the density and the coefficient of restitution.

The organization of the paper is as follows. In §2 the model kinetic equation is introduced and its derivation from the RET is briefly discussed. The model is particularized for steady simple shear flow in §3, where a method to obtain numerically the elements of the pressure tensor in the first Sonine approximation is discussed in detail. In the limit of small dissipation it is possible to derive explicit analytical expressions for these elements. Section 4 deals with the Monte Carlo simulation of the RET equation particularized for steady simple shear flow. The results are presented and discussed in §5, where a simplified expression for the pressure tensor is introduced and seen to agree well with the simulations. The one-particle distribution function is also considered. The rheological properties are compared with those derived from

the well-known theory developed by Lun *et al.* (1984), while a comparison with the maximum-entropy approximation for the distribution function is also carried out. Finally, §6 provides a short summary and conclusions.

2. Description of the model

The model kinetic equation we will use in the following was introduced as an approximate representation of the revised Enskog theory (RET) for a dense gas of smooth inelastic hard spheres of mass m and diameter σ. Inelasticity in collisions is introduced through a constant coefficient of normal restitution α. The RET gives an evolution equation for the single-particle distribution function, $f(\boldsymbol{r}, \boldsymbol{v}, t)$ (Brey *et al.* 1997*a*)

$$\left(\frac{\partial}{\partial t} + \boldsymbol{v}_1 \cdot \nabla_1\right) f(\boldsymbol{r}_1, \boldsymbol{v}_1, t) = \mathscr{J}_E[\boldsymbol{r}_1, \boldsymbol{v}_1 | f(t)], \tag{2.1}$$

where $\mathscr{J}_E$ is the Enskog collision operator

$$\mathscr{J}_E[\boldsymbol{r}_1, \boldsymbol{v}_1 | f(t)] = \sigma^2 \int \mathrm{d}\boldsymbol{v}_2 \int \mathrm{d}\widehat{\boldsymbol{\sigma}}\, \Theta(\boldsymbol{g} \cdot \widehat{\boldsymbol{\sigma}})(\boldsymbol{g} \cdot \widehat{\boldsymbol{\sigma}}) \left[\alpha^{-2} f^{(2)}(\boldsymbol{r}_1, \boldsymbol{r}_1 - \boldsymbol{\sigma}, \boldsymbol{v}_1', \boldsymbol{v}_2', t) \right.$$
$$\left. - f^{(2)}(\boldsymbol{r}_1, \boldsymbol{r}_1 + \boldsymbol{\sigma}, \boldsymbol{v}_1, \boldsymbol{v}_2, t)\right]. \tag{2.2}$$

Here,

$$f^{(2)}(\boldsymbol{r}_1, \boldsymbol{r}_2, \boldsymbol{v}_1, \boldsymbol{v}_2, t) = \chi[\boldsymbol{r}_1, \boldsymbol{r}_2 | n(t)] f(\boldsymbol{r}_1, \boldsymbol{v}_1, t) f(\boldsymbol{r}_2, \boldsymbol{v}_2, t), \tag{2.3}$$

with $\chi[\boldsymbol{r}_1, \boldsymbol{r}_2 | n(t)]$ being the equilibrium pair correlation function as a functional of the non-equilibrium density field

$$n(\boldsymbol{r}, t) = \int \mathrm{d}\boldsymbol{v}\, f(\boldsymbol{r}, \boldsymbol{v}, t). \tag{2.4}$$

Moreover, Θ is the Heaviside step function, $\widehat{\boldsymbol{\sigma}}$ is a unit vector, $\boldsymbol{\sigma} = \sigma\widehat{\boldsymbol{\sigma}}$, $\boldsymbol{g} = \boldsymbol{v}_1 - \boldsymbol{v}_2$ and

$$\boldsymbol{v}_1' = \boldsymbol{v}_1 - \frac{1+\alpha}{2\alpha}(\boldsymbol{g} \cdot \widehat{\boldsymbol{\sigma}})\widehat{\boldsymbol{\sigma}}, \tag{2.5a}$$

$$\boldsymbol{v}_2' = \boldsymbol{v}_2 + \frac{1+\alpha}{2\alpha}(\boldsymbol{g} \cdot \widehat{\boldsymbol{\sigma}})\widehat{\boldsymbol{\sigma}} \tag{2.5b}$$

are the precollisional velocities yielding $(\boldsymbol{v}_1, \boldsymbol{v}_2)$ as postcollisional ones. Balance equations for number of particles, momentum and energy are derived from (2.1) by multiplying by 1, $m\boldsymbol{v}_1$ and $m v_1^2/2$, respectively, and integrating over $\boldsymbol{v}_1$. Defining the flow velocity $\boldsymbol{u}(\boldsymbol{r}, t)$ and the local (granular) temperature $T(\boldsymbol{r}, t)$ in the standard way,

$$n(\boldsymbol{r}, t)\boldsymbol{u}(\boldsymbol{r}, t) = \int \mathrm{d}\boldsymbol{v}\, \boldsymbol{v} f(\boldsymbol{r}, \boldsymbol{v}, t), \tag{2.6}$$

$$\tfrac{3}{2} n(\boldsymbol{r}, t) T(\boldsymbol{r}, t) = \int \mathrm{d}\boldsymbol{v}\, \tfrac{1}{2} m V^2(\boldsymbol{r}, t) f(\boldsymbol{r}, \boldsymbol{v}, t), \tag{2.7}$$

where $\boldsymbol{V}(\boldsymbol{r}, t) = \boldsymbol{v} - \boldsymbol{u}(\boldsymbol{r}, t)$, results in

$$\frac{\partial n}{\partial t} + \nabla \cdot (n\boldsymbol{u}) = 0, \tag{2.8}$$

$$\frac{\partial \boldsymbol{u}}{\partial t} + \boldsymbol{u} \cdot \nabla \boldsymbol{u} + (mn)^{-1} \nabla \cdot \boldsymbol{P} = 0, \tag{2.9}$$

$$\frac{\partial T}{\partial t} + \boldsymbol{u} \cdot \nabla T + \frac{2}{3n} \left[\boldsymbol{P} : \nabla \boldsymbol{u} + \nabla \cdot \boldsymbol{q} + (1 - \alpha^2)\omega \right] = 0. \tag{2.10}$$

The expressions for the pressure tensor, $\boldsymbol{P}$, and the heat flux, $\boldsymbol{q}$, contain both 'kinetic' and 'collisional transfer' contributions,

$$\boldsymbol{P} = \boldsymbol{P}^k + \boldsymbol{P}^c, \quad \boldsymbol{q} = \boldsymbol{q}^k + \boldsymbol{q}^c. \tag{2.11}$$

They are given by

$$\boldsymbol{P}^k(\boldsymbol{r}, t) = \int \mathrm{d}\boldsymbol{v} m \boldsymbol{V} \boldsymbol{V} f(\boldsymbol{r}, \boldsymbol{v}, t), \tag{2.12}$$

$$\boldsymbol{q}^k(\boldsymbol{r}, t) = \int \mathrm{d}\boldsymbol{v} \frac{m}{2} V^2 \boldsymbol{V} f(\boldsymbol{r}, \boldsymbol{v}, t), \tag{2.13}$$

$$\boldsymbol{P}^c(\boldsymbol{r}, t) = \frac{1 + \alpha}{4} m\sigma^3 \int \mathrm{d}\boldsymbol{v}_1 \int \mathrm{d}\boldsymbol{v}_2 \int \mathrm{d}\widehat{\boldsymbol{\sigma}}\, \Theta(\boldsymbol{g} \cdot \widehat{\boldsymbol{\sigma}})(\boldsymbol{g} \cdot \widehat{\boldsymbol{\sigma}})^2 \widehat{\boldsymbol{\sigma}}\widehat{\boldsymbol{\sigma}} F(\boldsymbol{r}, \boldsymbol{\sigma}, \boldsymbol{v}_1, \boldsymbol{v}_2, t), \tag{2.14}$$

$$\boldsymbol{q}^c(\boldsymbol{r}, t) = \frac{1 + \alpha}{4} m\sigma^3 \int \mathrm{d}\boldsymbol{v}_1 \int \mathrm{d}\boldsymbol{v}_2 \int \mathrm{d}\widehat{\boldsymbol{\sigma}}\, \Theta(\boldsymbol{g} \cdot \widehat{\boldsymbol{\sigma}})(\boldsymbol{g} \cdot \widehat{\boldsymbol{\sigma}})^2 (\widetilde{\boldsymbol{G}} \cdot \widehat{\boldsymbol{\sigma}})\widehat{\boldsymbol{\sigma}} F(\boldsymbol{r}, \boldsymbol{\sigma}, \boldsymbol{v}_1, \boldsymbol{v}_2, t). \tag{2.15}$$

In the above expressions, $\widetilde{\boldsymbol{G}} = \frac{1}{2}(\boldsymbol{v}_1 + \boldsymbol{v}_2) - \boldsymbol{u}$ and we have introduced

$$F(\boldsymbol{r}, \boldsymbol{\sigma}, \boldsymbol{v}_1, \boldsymbol{v}_2, t) = \int_0^1 \mathrm{d}\lambda \; f^{(2)}(\boldsymbol{r} - (1 - \lambda)\boldsymbol{\sigma}, \boldsymbol{r} + \lambda\boldsymbol{\sigma}, \boldsymbol{v}_1, \boldsymbol{v}_2, t). \tag{2.16}$$

A derivation of (2.14)–(2.16) for the elastic limit $\alpha = 1$ is given in Appendix B of Santos *et al.* (1998). The generalization to arbitrary coefficient of restitution is straightforward. Finally, the term $(1 - \alpha^2)\omega$ in (2.10) describes the rate of energy dissipation in collisions due to inelasticity. The explicit expression for ω is

$$\omega(\boldsymbol{r}, t) = \frac{m}{8}\sigma^2 \int \mathrm{d}\boldsymbol{v}_1 \int \mathrm{d}\boldsymbol{v}_2 \int \mathrm{d}\widehat{\boldsymbol{\sigma}}\Theta(\boldsymbol{g} \cdot \widehat{\boldsymbol{\sigma}})(\boldsymbol{g} \cdot \widehat{\boldsymbol{\sigma}})^3 f^{(2)}(\boldsymbol{r}, \boldsymbol{r} + \boldsymbol{\sigma}, \boldsymbol{v}_1, \boldsymbol{v}_2, t). \tag{2.17}$$

The complexity of the RET has limited its use to states near equilibrium. Even in the elastic limit $\alpha = 1$, almost nothing is known about solutions corresponding to far from equilibrium situations. This has lead to the introduction of model kinetic equations, in which the collision operator is replaced by a simpler form that, nevertheless, retains the relevant physical and mathematical properties of the original one. Here we will use a model that has been proposed very recently (Dufty, Brey & Santos 1997). The model has already been applied to the study of both dissipative systems in the low-density, or Boltzmann, limit (Brey, Ruiz-Montero & Moreno 1997*b*) and dense systems in the elastic limit (Santos *et al.* 1998). In this paper a dense dissipative system will be considered.

The starting point for the formulation of the model kinetic equation is to represent the collision operator $\mathscr{J}_E$ as an expansion in a complete set of velocity polynomials, with a scalar product weighted with the local equilibrium distribution. The functional form of the contribution in the subspace spanned by 1, $\boldsymbol{v}$, and v^2 is retained exactly. On the other hand, the contribution from the subspace orthogonal to that is approximated by a single relaxation term plus a correction that takes into account that the Enskog collision operator does not vanish for the local equilibrium distribution function. The details of the reasoning and calculations leading to the model equation have been

presented elsewhere (Dufty *et al.* 1997*b*; Santos *et al.* 1998). Therefore, we only report here the resulting equation:

$$\left(\frac{\partial}{\partial t} + \boldsymbol{v} \cdot \nabla\right) f = -\zeta \left(f - f_\ell\right) + \frac{1}{T} f_\ell \left[\boldsymbol{A} : \boldsymbol{D}(V) + \boldsymbol{B} \cdot \boldsymbol{S}(V)\right] - \frac{1}{nT} f_\ell \left\{ V\nabla : \boldsymbol{P}^c \right.$$
$$\left. + \left(\frac{m}{3T} V^2 - 1\right) \left[\nabla \cdot \boldsymbol{q}^c + \boldsymbol{P}^c : \nabla \boldsymbol{u} + (1 - \alpha^2)\omega\right] \right\}, \quad (2.18)$$

where

$$f_\ell(\boldsymbol{r}, \boldsymbol{v}, t) = n \left(\frac{m}{2\pi T}\right)^{1/2} \exp\left(-mV^2/2T\right) \quad (2.19)$$

is the local equilibrium distribution function and

$$\boldsymbol{D}(V) = m \left(VV - \tfrac{1}{3} V^2 \boldsymbol{I}\right), \quad \boldsymbol{S}(V) = \left(\tfrac{1}{2} mV^2 - \tfrac{5}{2} T\right) V, \quad (2.20)$$

$$\boldsymbol{A} = \frac{1}{2nT} \int \mathrm{d}V \, \boldsymbol{D}(V) \mathscr{J}_E[f_\ell], \quad \boldsymbol{B} = \frac{2m}{5nT^2} \int \mathrm{d}V \, \boldsymbol{S}(V) \mathscr{J}_E[f_\ell]. \quad (2.21)$$

In (2.20) $\boldsymbol{I}$ denotes the unit tensor. The model equation (2.18) contains the effective collision frequency ζ. In practical applications it can be fixed by requiring that the model reproduces some quantitative property of the (exact) Enskog equation, for instance the value of a given transport coefficient. Let us stress that the model not only reproduces by construction the form of the exact balance equations (2.8)–(2.10) following from the RET, but the expressions for the fluxes and the energy source terms are given by the same functionals of the distribution function as in the RET, cf. (2.14)–(2.17).

3. Solution of the model for simple shear flow

As stated in the Introduction, simple shear flow is characterized by a linear profile of the flow velocity: $\boldsymbol{u}(\boldsymbol{r}) = \boldsymbol{a} \cdot \boldsymbol{r}$, where the elements of the tensor $\boldsymbol{a}$ are $a_{ij} = a\delta_{ix}\delta_{jy}$, a being the constant shear rate. Otherwise, the number density n and the granular temperature T are uniform. The temperature changes in time due to the competition between two mechanisms: on the one hand, viscous heating and, on the other hand, energy dissipation in collisions. In the steady state, both mechanisms cancel each other and the temperature remains constant. In that case, according to the energy balance equation (2.10), the shear stress P_{xy} and the sink term ω are related by

$$aP_{xy} = -(1 - \alpha^2)\omega. \quad (3.1)$$

This steady simple shear flow is the problem we want to analyse by means of the kinetic model described in §2, as well as by performing Monte Carlo simulations of the Enskog equation.

All the spatial dependence of the velocity distribution function occurs through the peculiar velocity $\boldsymbol{V} = \boldsymbol{v} - \boldsymbol{u}(\boldsymbol{r})$: $f(\boldsymbol{r}, \boldsymbol{v}) \to f(\boldsymbol{V})$. Consequently, the kinetic model (2.18) becomes

$$\left(\zeta - aV_y \frac{\partial}{\partial V_x}\right) f(V) = \zeta f_\ell(V) \left[1 + \frac{1}{nT\zeta} \left(\frac{m}{3T} V^2 - 1\right) P_{xy}^k a + \frac{1}{T\zeta} \boldsymbol{A} : \boldsymbol{D}(V)\right]$$
$$\equiv \zeta \widetilde{f}_\ell(V), \quad (3.2)$$

where we have taken into account (3.1), that the pressure tensor is uniform and

that, by symmetry reasons, the heat flux $\boldsymbol{q}$ and the vector $\boldsymbol{B}$ vanish. For the collision frequency we will take the following:

$$\zeta = \tfrac{16}{5}\pi^{1/2}n\sigma^2\chi(T/m)^{1/2}, \tag{3.3}$$

so that the Enskog shear viscosity coefficient for elastic spheres is recovered (Dufty *et al.* 1997). The solution to (3.2) can be formally written as

$$f(\boldsymbol{V}) = \int_0^\infty \mathrm{d}s\, \mathrm{e}^{-s}\widetilde{f}_\ell\left(\boldsymbol{V} + \frac{s}{\zeta}\boldsymbol{a}\cdot\boldsymbol{V}\right). \tag{3.4}$$

This solution is not complete, since we need to know the quantities T, P_{xy}^k, and A_{ij} for given values of a, n, and α. The tensor A_{ij} is determined entirely by the local equilibrium distribution f_ℓ, cf. (2.21), so that it only depends on T. Its non-zero elements are

$$A_{xy} = -\frac{4\pi}{15}(T/m)^{1/2}n\sigma^2\chi\widetilde{a}\frac{1+\alpha}{2}\left[\tfrac{1}{2}(3\alpha-1)+\tfrac{1}{7}(1+\alpha)\widetilde{a}^2\right], \tag{3.5}$$

$$A_{xx} = A_{yy} = -\tfrac{1}{2}A_{zz}$$
$$= (T/m)^{1/2}n\sigma^2\chi\int \mathrm{d}\widehat{\boldsymbol{\sigma}}(\widehat{\sigma}_x^2 - \tfrac{1}{3})\widetilde{a}\widehat{\sigma}_x\widehat{\sigma}_y\frac{1+\alpha}{2}\left\{\frac{(1+\alpha)}{\pi^{1/2}}\widetilde{a}\widehat{\sigma}_x\widehat{\sigma}_y\mathrm{e}^{-\widetilde{a}^2\widehat{\sigma}_x^2\widehat{\sigma}_y^2}\right.$$
$$\left.+\operatorname{erf}(\widetilde{a}\widehat{\sigma}_x\widehat{\sigma}_y)\left[\tfrac{1}{2}(3\alpha-1)+(1+\alpha)\widetilde{a}^2\widehat{\sigma}_x^2\widehat{\sigma}_y^2\right]-\frac{1}{\pi^{1/2}}(1-\alpha)\frac{\mathrm{e}^{-\widetilde{a}^2\widehat{\sigma}_x^2\widehat{\sigma}_y^2}}{\widetilde{a}\widehat{\sigma}_x\widehat{\sigma}_y}\right\}, \tag{3.6}$$

where erf denotes the error function, $\widetilde{a} \equiv \tfrac{1}{2}a\sigma(m/T)^{1/2}$ and we have taken into account that $\chi(n)$ is a constant in our problem. The relationship between P_{xy}^k and T is easily found by multiplying both sides of (3.4) by mV_xV_y and integrating over velocity space. The result is

$$P_{xy}^k = -nT\frac{a}{\zeta}\left(1 + \frac{2a}{3nT\zeta}P_{xy}^k - 2\frac{A_{xy}}{a} + 2\frac{A_{xx}}{\zeta}\right). \tag{3.7}$$

In order to close the problem, we need an extra condition. This is provided by (3.1), where P_{xy}^c and ω are determined by replacing f by the right-hand side of (3.4) in the equations

$$P_{ij}^c = \frac{1+\alpha}{4}m\sigma^3\chi\int \mathrm{d}\widehat{\boldsymbol{\sigma}}\widehat{\sigma}_i\widehat{\sigma}_j\int \mathrm{d}\boldsymbol{V}_1\int \mathrm{d}\boldsymbol{V}_2\Theta(\widehat{\boldsymbol{\sigma}}\cdot\boldsymbol{g})(\widehat{\boldsymbol{\sigma}}\cdot\boldsymbol{g})^2 f(\boldsymbol{V}_1+\boldsymbol{a}\cdot\boldsymbol{\sigma})f(\boldsymbol{V}_2), \tag{3.8}$$

$$\omega = \frac{m\sigma^2}{8}\chi\int \mathrm{d}\widehat{\boldsymbol{\sigma}}\int \mathrm{d}\boldsymbol{V}_1\int \mathrm{d}\boldsymbol{V}_2\Theta(\widehat{\boldsymbol{\sigma}}\cdot\boldsymbol{g})(\widehat{\boldsymbol{\sigma}}\cdot\boldsymbol{g})^3 f(\boldsymbol{V}_1+\boldsymbol{a}\cdot\boldsymbol{\sigma})f(\boldsymbol{V}_2), \tag{3.9}$$

which follow from (2.14) and (2.17), respectively. Once P_{xy}^k and T are known, the remaining elements of the pressure tensor can be obtained. Their kinetic parts are

$$P_{xx}^k = nT\left(1 - \frac{4a}{3nT\zeta}P_{xy}^k + 2\frac{A_{xx}}{\zeta}\right), \tag{3.10}$$

$$P_{yy}^k = nT\left(1 + \frac{2a}{3nT\zeta}P_{xy}^k + 2\frac{A_{xx}}{\zeta}\right), \tag{3.11}$$

$$P_{zz}^k = nT\left(1 + \frac{2a}{3nT\zeta}P_{xy}^k - 4\frac{A_{xx}}{\zeta}\right). \tag{3.12}$$

The corresponding collisional parts are evaluated using (3.8).

Although the problem of solving the kinetic model for steady simple shear flow is closed, the numerical integrations in (3.8) and (3.9) are very intricate. Thus, from a practical point of view, it is more convenient to take the first Sonine approximation (Chapman & Cowling 1970) for f in those equations, rather than the solution (3.4). This strategy proved to be useful in the elastic case (Santos *et al.* 1998) and, as will be seen in §5, the agreement with Monte Carlo simulations is also good in the inelastic case. In the first Sonine approximation, $f(V) \to f_\ell(V)[1 + \mathbf{C} : \mathbf{D}(V)/2T]$, where

$$\mathbf{C} = \frac{1}{nT}\mathbf{P}^k - \mathbf{I}. \tag{3.13}$$

With this approximation, the evaluation of P_{ij}^c and ω is similar to that of the tensor A_{ij}. The result is

$$P_{ij}^c = -\frac{1+\alpha}{4}nTn^*\chi \int \mathrm{d}\hat{\boldsymbol\sigma}\,\hat{\sigma}_i\hat{\sigma}_j \left\{ \frac{2}{\pi^{1/2}}\tilde{a}\hat{\sigma}_x\hat{\sigma}_y\mathrm{e}^{-\tilde{a}^2\hat{\sigma}_x^2\hat{\sigma}_y^2} - \left(1 + 2\tilde{a}^2\hat{\sigma}_x^2\hat{\sigma}_y^2\right)\mathrm{erfc}\left(\tilde{a}\hat{\sigma}_x\hat{\sigma}_y\right) \right.$$
$$\left. - \left(\hat{\boldsymbol\sigma}\hat{\boldsymbol\sigma} - \tfrac{1}{3}\mathbf{I}\right):\mathbf{C}\,\mathrm{erfc}\left(\tilde{a}\hat{\sigma}_x\hat{\sigma}_y\right) - \tfrac{1}{8}\left[\left(\hat{\boldsymbol\sigma}\hat{\boldsymbol\sigma} - \tfrac{1}{3}\mathbf{I}\right):\mathbf{C}\right]^2 \frac{2}{\pi^{1/2}}\tilde{a}\hat{\sigma}_x\hat{\sigma}_y\mathrm{e}^{-\tilde{a}^2\hat{\sigma}_x^2\hat{\sigma}_y^2} \right\}, \tag{3.14}$$

$$\omega = nTn\sigma^2\chi(T/m)^{1/2} \int \mathrm{d}\hat{\boldsymbol\sigma} \left\{ \frac{1}{2\pi^{1/2}}\left(1 + \tilde{a}^2\hat{\sigma}_x^2\hat{\sigma}_y^2\right)\mathrm{e}^{-\tilde{a}^2\hat{\sigma}_x^2\hat{\sigma}_y^2} \right.$$
$$+ \tfrac{1}{4}\left(3 + 2\tilde{a}^2\hat{\sigma}_x^2\hat{\sigma}_y^2\right)\tilde{a}\hat{\sigma}_x\hat{\sigma}_y\mathrm{erf}\left(\tilde{a}\hat{\sigma}_x\hat{\sigma}_y\right)$$
$$+ \tfrac{3}{2}\left(\hat{\boldsymbol\sigma}\hat{\boldsymbol\sigma} - \tfrac{1}{3}\mathbf{I}\right):\mathbf{C}\left[\frac{1}{2\pi^{1/2}}\mathrm{e}^{-\tilde{a}^2\hat{\sigma}_x^2\hat{\sigma}_y^2} + \tfrac{1}{2}\tilde{a}\hat{\sigma}_x\hat{\sigma}_y\mathrm{erf}\left(\tilde{a}\hat{\sigma}_x\hat{\sigma}_y\right)\right]$$
$$\left. + \tfrac{3}{32}\left[\left(\hat{\boldsymbol\sigma}\hat{\boldsymbol\sigma} - \tfrac{1}{3}\mathbf{I}\right):\mathbf{C}\right]^2 \frac{1}{\pi^{1/2}}\mathrm{e}^{-\tilde{a}^2\hat{\sigma}_x^2\hat{\sigma}_y^2} \right\}. \tag{3.15}$$

Here, $n^* \equiv n\sigma^3$ is the reduced number density. It is related to the solid fraction v by $v = \frac{1}{6}\pi n^*$. In summary, (3.7) and (3.10)–(3.12) allow one to express $\mathbf{C}$ as a function of T; when (3.14) and (3.15) are used in (3.1), one gets a *closed* equation for the temperature T, that can be solved numerically.

It is interesting to consider the limit of low dissipation, in which case it is possible to get analytical results and the Sonine approximation is not needed. To that end, we introduce the perturbation parameter $\epsilon \equiv 1 - \alpha^2$ and perform a power series expansion around $\epsilon = 0$. The details of the calculation are presented in the Appendix and here we only give the final results. First, the expression for the granular temperature is given through the ratio a/ζ (which measures the shear rate in units of the collision frequency) as

$$\frac{a}{\zeta} = \bar{a}_1(1 - \alpha^2)^{1/2} + \bar{a}_3(1 - \alpha^2)^{3/2} + \cdots. \tag{3.16}$$

Next, the elements of the pressure tensor can be written as

$$\frac{1}{nT}P_{xx} = 1 + \frac{2\pi}{3}n^*\chi + \left(P_{xx,2}^k + P_{xx,2}^c\right)\bar{a}_1^2(1 - \alpha^2) + \cdots, \tag{3.17}$$

$$\frac{1}{nT}P_{yy} = 1 + \frac{2\pi}{3}n^*\chi + \left(P_{yy,2}^k + P_{yy,2}^c\right)\bar{a}_1^2(1 - \alpha^2) + \cdots, \tag{3.18}$$

$$\frac{1}{nT}P_{zz} = 1 + \frac{2\pi}{3}n^*\chi + \left(P_{zz,2}^k + P_{zz,2}^c\right)\bar{a}_1^2(1-\alpha^2) + \cdots, \tag{3.19}$$

$$\frac{\zeta}{a}\frac{1}{nT}P_{xy} = P_{xy,1}^k + P_{xy,1}^c + \left(P_{xy,3}^k + P_{xy,3}^c\right)\bar{a}_1^2(1-\alpha^2) + \cdots. \tag{3.20}$$

In these equations, $\bar{a}_1$, $\bar{a}_3$, $P_{ij,\ell}^k$, and $P_{ij,\ell}^c$ are dimensionless coefficients that depend on the density and are explicitly given in the Appendix.

In what follows, we will use the Carnahan & Starling (1969) approximation for the density dependence of the pair correlation function at contact:

$$\chi(v) = \frac{1 - \frac{1}{2}v}{(1-v)^3}. \tag{3.21}$$

Of course, one could take any other approximation for χ since the simulation and theory results depend on density only through the product $v\chi(v)$.

4. Monte Carlo simulation

Recently, Montanero & Santos (1996, 1997a) have proposed a simulation Monte Carlo (ESMC) algorithm that solves the Enskog equation for a system of elastic hard spheres, in the same spirit as the well-known DSMC method for solving the Boltzmann equation (Bird 1994). The extension of the ESMC method to deal with inelastic collisions is straightforward (Brey *et al.* 1997a). In the particular case of simple shear flow, the simulation method is especially easy to implement, due to the fact that this state is homogeneous in the local Lagrangian frame. This is an important advantage with respect to molecular dynamics simulations. In contrast, the restriction to this quasi-homogeneous state prevents us from analysing the possible instability of simple shear flow or the formation of microstructures.

The ESMC method, as applied to simple shear flow, proceeds as follows (Montanero & Santos 1997b). The one-particle distribution function is represented by the peculiar velocities $\{V_r\}$ of a sample of N 'simulated' particles:

$$f(V,t) \to n\frac{1}{N}\sum_{r=1}^{N}\delta(V - V_r(t)). \tag{4.1}$$

The velocities are updated at integer times $t = \Delta t, 2\Delta t, 3\Delta t, \ldots$, where the time step Δt is much smaller than the mean free time and the inverse shear rate. This is done in two stages: free streaming and collisions. In the local Lagrangian frame, the particles are subjected to the action of a non-conservative inertial force $F = -m\mathbf{a} \cdot V$. This is represented by the second term on the left-hand side of (3.2). Thus, the free-streaming stage consists of making $V_r \to V_r - \mathbf{a} \cdot V_r\Delta t$. In the collision stage, a sample of $\frac{1}{2}Nw_{\max}$ pairs is chosen at random with equiprobability, where $w_{\max}$ is an upper bound estimate of the probability that a particle collides in the time interval between t and $t + \Delta t$. For each pair rs belonging to this sample, the following steps are taken: (1) a given direction $\hat{\boldsymbol{\sigma}}_{rs}$ is chosen at random with equiprobability; (2) the collision between particles r and s is accepted with a probability equal to $\Theta(\hat{\boldsymbol{\sigma}}_{rs} \cdot \mathbf{g}_{rs})w_{rs}/w_{\max}$, where $w_{rs} = 4\pi\sigma^2\chi n\hat{\boldsymbol{\sigma}}_{rs} \cdot \mathbf{g}_{rs}\Delta t$ and $\mathbf{g}_{rs} = V_r - V_s - \sigma\mathbf{a} \cdot \hat{\boldsymbol{\sigma}}_{rs}$; (3) if the collision is accepted, postcollisional velocities are assigned to both particles: $V_r \to V_r - \frac{1}{2}(1+\alpha)(\hat{\boldsymbol{\sigma}}_{rs} \cdot \mathbf{g}_{rs})\hat{\boldsymbol{\sigma}}_{rs}$, $V_s \to V_s + \frac{1}{2}(1 + \alpha)(\hat{\boldsymbol{\sigma}}_{rs} \cdot \mathbf{g}_{rs})\hat{\boldsymbol{\sigma}}_{rs}$. In the case that in one of the collisions $w_{rs} > w_{\max}$, the estimate of $w_{\max}$ is updated as $w_{\max} = w_{rs}$. Typically, the fraction of particles that change their velocities due to collisions is of the order of $w_{\max}$. This particularization
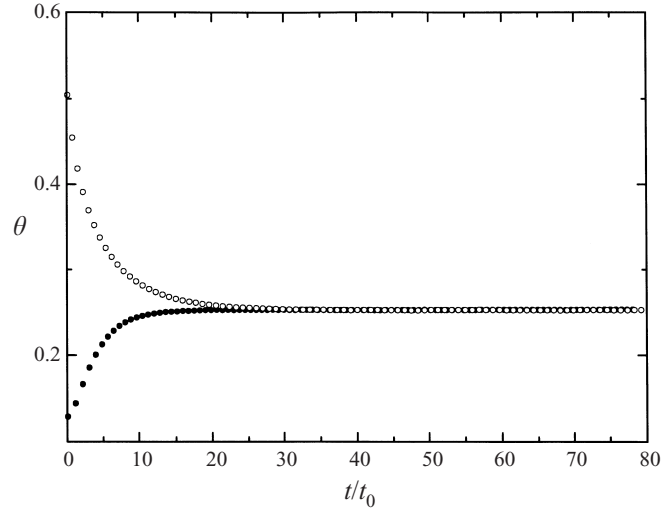
FIGURE 1. Time evolution of the reduced temperature θ, as obtained from Monte Carlo simulation of the Enskog equation, starting from two different initial conditions. The coefficient of restitution is $\alpha = 0.6$ and the solid fraction is $v = 0.25$; t_0 represents the Enskog mean free time corresponding to the initial temperature.

of the ESMC method to simple shear flow is equivalent to the simulation method proposed by Hopkins & Shen (1992).

In the course of the simulations, one evaluates the kinetic and collisional transfer contributions to the pressure tensor. They are given as

$$\mathbf{P}^k = \frac{mn}{N} \sum_{r=1}^{N} \mathbf{V}_r \mathbf{V}_r, \tag{4.2}$$

$$\mathbf{P}^c = \frac{mn}{N} \frac{(1+\alpha)\sigma}{2\Delta t} \sum_{rs}^{\dagger} (\widehat{\boldsymbol{\sigma}}_{rs} \cdot \boldsymbol{g}_{rs}) \widehat{\boldsymbol{\sigma}}_{rs} \widehat{\boldsymbol{\sigma}}_{rs}, \tag{4.3}$$

where the dagger means that the summation is restricted to the accepted collisions. The granular temperature is obtained from the trace of $\mathbf{P}^k$. To improve the statistics, the results are averaged over a number $\mathcal{N}$ of independent realizations or replicas. In the simulations reported in this paper, we have considered $N = 10^5$ particles, $\mathcal{N} = 20$ replicas and a time step $\Delta t = 10^{-2}\lambda/(2T/m)^{1/2}$, where $\lambda = (\sqrt{2}\pi n\sigma^2\chi)^{-1}$ is the mean free path. Notice that Δt depends on time through the temperature.

As usual (Lun *et al.* 1984; Campbell 1989, 1990; Lun 1996), one defines a dimensionless stress tensor τ_{ij} and a dimensionless temperature θ as

$$\tau_{ij} = \frac{|P_{ij}|}{\rho_p \sigma^2 a^2}, \tag{4.4}$$

$$\theta = \frac{T}{m\sigma^2 a^2}, \tag{4.5}$$

where $\rho_p = 6m/\pi\sigma^3$ is the particle mass density. In the steady state, these quantities are independent of the initial state, the shear rate a, the particle size σ and the particle mass m, for given values of the coefficient of restitution α and the solid fraction v. This is illustrated in figure 1, where the reduced temperature θ is plotted as a function
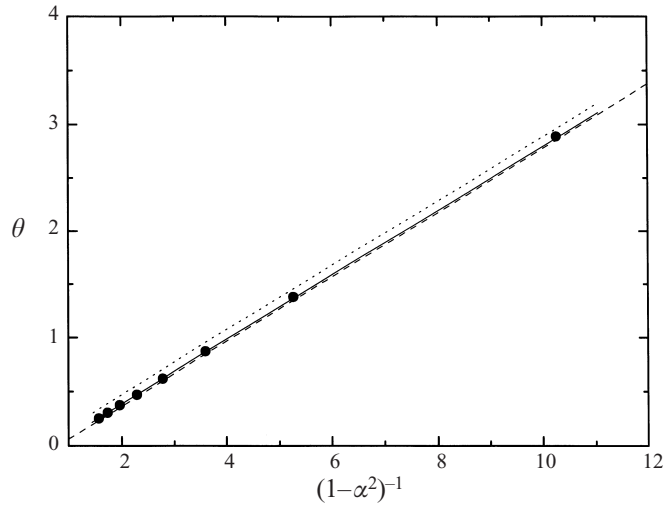
FIGURE 2. Plot of the reduced temperature θ versus the parameter $(1-\alpha^2)^{-1}$ for $v = 0.25$, as obtained from simulation (circles), the numerical solution of the kinetic model (solid line), the simplified solution of the model (dashed line) and the LSJC theory (dotted line).

of time for $\alpha = 0.6$ and $v = 0.25$, starting from two different initial conditions. It is evident that after a transient stage, a common steady state is reached. The duration of the transient stage is typically 30 collisions per particle.

5. Results

In this Section we will explore the dependence of τ_{ij} and θ on the coefficient of restitution α and the solid fraction v. We will compare the results obtained from Monte Carlo simulations with those from the kinetic model discussed in §2 and §3 and with the well-known theory of Lun *et al.* (1984) (LSJC). In the latter theory, an approach close to the Chapman–Enskog method is used, so that it is more justified in the 'nearly elastic' case.

First, we shall investigate the dependence of the relevant quantities on α for a given density. Recently, Goldhirsch & Tan (1996) have performed molecular dynamics simulations of a dilute system of smooth inelastic disks and have found that the reduced temperature θ can be closely fitted by a linear function of $(1-\alpha^2)^{-1}$. The same result has been obtained from the solution of the kinetic model in the low-density limit by Brey *et al.* (1997b). Here we have observed the same behaviour for a finite density, both from the simulations and from the kinetic theory analyses. As an illustrative example, we consider $v = 0.25$. At this density, in the elastic case, the collisional contribution to the pressure is about twice the kinetic contribution. Figure 2 shows θ versus $(1-\alpha^2)^{-1}$ as obtained from the simulations (circles), from the numerical solution of the model (solid line), as described in §3, and from the LSJC theory (dotted line). It is clear that the model has an excellent agreement with the simulation results and also that θ is practically linear in $(1-\alpha^2)^{-1}$. Thus, a very good approximation is

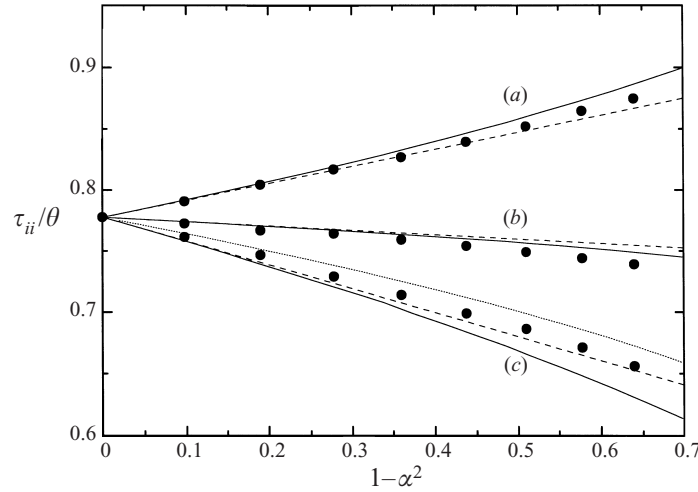$$\theta(v, \alpha) = \frac{\theta_1(v)}{1-\alpha^2} + \theta_2(v). \qquad (5.1)$$

FIGURE 3. Plot of (a) τ_{xx}/θ, (b) τ_{yy}/θ and (c) τ_{zz}/θ versus $1-\alpha^2$ for $v = 0.25$. Symbols and lines have the same meaning as in figure 2. Notice that in the LSJC theory the normal stresses are isotropic.

Consequently, the coefficients $\theta_{1,2}(v)$ in the model can be exactly obtained by comparing the low-dissipation behaviour of (5.1) with (3.16). The results are

$$\theta_1 = \frac{25\pi}{9216v^2\chi^2\bar{a}_1^2}, \tag{5.2}$$

$$\theta_2 = -\frac{25\pi\bar{a}_3}{4608v^2\chi^2\bar{a}_1^3}. \tag{5.3}$$

The function given by (5.1)–(5.3) is also plotted in figure 2 (dashed line). The fact that the dashed and the solid lines do not coincide exactly is due to the Sonine approximation used to evaluate P_{ij}^c and ω in the numerical solution of the model. While this approximation is consistent with the exact $\bar{a}_1$, it gives a small deviation from the exact $\bar{a}_3$. The LSJC theory overestimates the temperature, but it is also consistent with a linear behaviour of the form (5.1). While the slope is exactly given by (5.2), the line is shifted with respect to the simulation results. This is because the LSJC theory is based on a first-order (Navier–Stokes) Chapman–Enskog expansion, while the correct determination of θ_2 requires going to third-order (super-Burnett).

Apart from the temperature, the non-zero elements of the stress tensor, namely τ_{xx}, τ_{yy}, τ_{zz} and $\tau_{xy} = \tau_{yx}$ are the most relevant quantities. We have observed that the dependence of these elements on the coefficient of restitution is not well fitted by relations similar to that of (5.1). On the other hand, the solution of the model in the low-density regime (Brey *et al.* 1997*b*) predicts that the ratios τ_{ii}/θ, $i = x, y, z$, and $\tau_{xy}/\theta^{1/2}$ are linear functions of $1 - \alpha^2$. Notice that $\tau_{ii}/\theta = vP_{ii}/nT$ and $\tau_{xy}/\theta^{1/2} = -(5\pi^{1/2}/96\chi)(\zeta/nTa)P_{xy}$. A natural question is whether the above simple behaviours can be extended to dense systems. In figures 3 and 4 we plot τ_{ii}/θ and $\tau_{xy}/\theta^{1/2}$, respectively, as functions of $1 - \alpha^2$ for $v = 0.25$. The agreement of the model predictions with the simulation data is generally good, although the discrepancies are larger than in the case of the temperature. We observe that the plotted quantities are indeed *quasi*-linear functions, especially in the case of the simulation results. Consequently, one can obtain a good approximation by considering the low-dissipation expansions (3.17)–(3.20) truncated to the order $1 - \alpha^2$. These
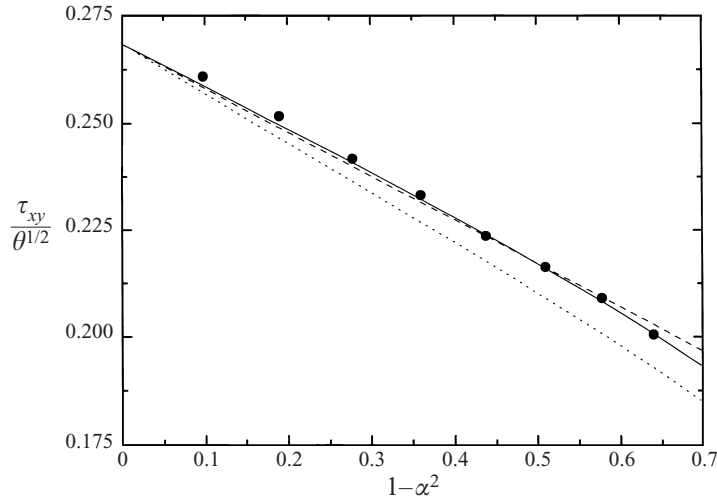
Figure 4. The same as in figure 3 but for $\tau_{xy}/\theta^{1/2}$.

truncated expansions are also shown in figures 3 and 4. It is interesting to remark that the truncated expansions for τ_{xx}/θ and τ_{zz}/θ agree with the simulation even better than the numerical solution of the model. In contrast, the LSJC theory, that predicts the absence of normal stress differences, i.e. $\tau_{xx} = \tau_{yy} = \tau_{zz}$, gives a poor agreement for the diagonal elements of the pressure tensor; by accident, it captures the general trend of τ_{zz}/θ. In the case of the off-diagonal element, the LSJC theory underestimates the ratio $\tau_{xy}/\theta^{1/2}$.

The above discussion shows that the granular temperature and the stress tensor have a dependence on α that can be well fitted by simple forms. In addition, the kinetic model exhibits a good agreement with the simulation results. Both facts suggest that a good approximation can be obtained by using the analytical solution of the model for low dissipation. This approach gives explicit expressions for the main quantities as functions of the solid fraction and the coefficient of restitution and also avoids the need to numerically solve the model. Consequently, we propose that the temperature is given by (5.1)–(5.3) and the stress tensor is given by

$$\tau_{ii}(\nu,\alpha) = \theta(\nu,\alpha)\nu\left[1 + 4\nu\chi + \left(P_{ii,2}^k + P_{ii,2}^c\right)\bar{a}_1^2(1-\alpha^2)\right], \tag{5.4}$$

$$\tau_{xy}(\nu,\alpha) = -\left[\theta(\nu,\alpha)\right]^{1/2}\frac{5\pi^{1/2}}{96\chi}\left[P_{xy,1}^k + P_{xy,1}^c + \left(P_{xy,3}^k + P_{xy,3}^c\right)\bar{a}_1^2(1-\alpha^2)\right]. \tag{5.5}$$

The collisional parts τ_{ij}^c are obtained by removing $P_{ij,1}^k$ and $P_{ij,2}^k$ in equations (5.4) and (5.5).

In figures 2–4 we have seen that (5.1)–(5.5) reproduce fairly well the simulation data for a solid fraction $\nu = 0.25$ and for a wide range of values of α. As a complement, let us see whether the same applies for all the densities. Figures 5, 6(a–d) and 7(a–d) show θ, τ_{ij} and their collisional part τ_{ij}^c, respectively, as functions of ν for $\alpha = 0.8, 0.6$ and 0.4. Figure 5 shows that the temperature predicted by our model in the approximation (5.1)–(5.3) has a very good agreement with the simulation data. On the other hand, the discrepancies increase as the dissipation increases. As already said in connection with figure 2, the LSJC theory overestimates the value of the granular temperature. However, its relative deviation decreases with density; at $\alpha = 0.8$, for
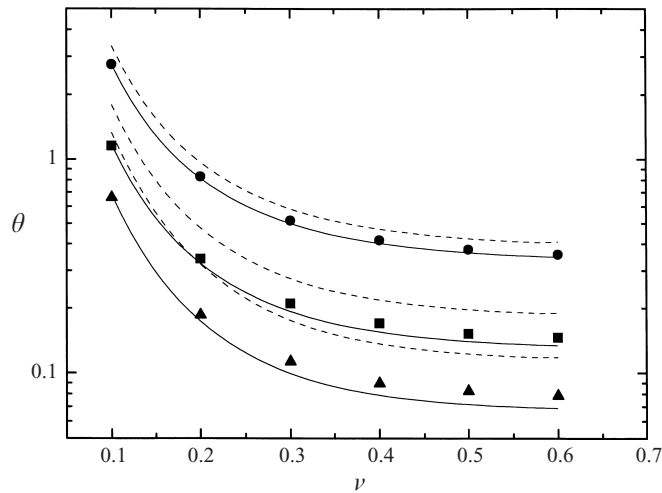
FIGURE 5. Plot of the reduced temperature θ as a function of the solid fraction v for $\alpha = 0.8$ (circles), $\alpha = 0.6$ (squares) and $\alpha = 0.4$ (triangles). Symbols refer to simulation results, the solid lines correspond to the simplified solution of the kinetic model and the dashed lines are the LSJC predictions.

instance, the relative deviation of the LSJC temperature from simulation goes from 21% at $v = 0.1$ to 14% at $v = 0.6$.

Concerning the elements of the stress tensor, figures 6(*a–d*) and 7(*a–d*) show that the predictions (5.4) and (5.5) of the simplified model are again in a good agreement with the simulation data, both for the total and the collisional contributions. This agreement is especially remarkable in the case of the shear stress τ_{xy}, which is the most important quantity in the simple shear flow problem. In the case of the diagonal elements, the model tends to underestimate their values with respect to the simulation data, although this is only noticeable for the smallest coefficient of restitution considered ($\alpha = 0.4$). The LSJC theory gives a good prediction of τ_{xy} for large densities and reproduces quite well the simulation values of τ_{xx}. Nevertheless, since this theory fails to account for normal stress effects, the disagreement for the other two diagonal elements is significant, especially for low densities and/or large dissipation.

In figure 8(*a–c*) we plot the ratios τ_{xx}/τ_{yy}, τ_{zz}/τ_{yy} and τ_{xy}/τ_{yy}. The agreement of the simplified model with the simulation results is very good for $\alpha = 0.8$ and mainly qualitative for $\alpha = 0.4$. As observed by Campbell (1989) and Hopkins & Shen (1992), the shear-plane normal stresses (τ_{xx} and τ_{yy}) tend to coincide when the solid fraction increases, while the out-of-shear-plane normal stress (τ_{zz}) tends to deviate from τ_{yy}. It is interesting to point out that the kinetic model predicts that $\tau_{zz}/\tau_{yy} \to 1$ in the limit $v \to 0$, while our simulation results, in agreement with those of Hopkins & Shen (1992), indicate that τ_{zz} is slightly larger than τ_{yy} in that limit. Figure 8(*c*) shows that the friction coefficient τ_{xy}/τ_{yy} first decreases with the solid fraction and then reaches a practically constant value (Campbell 1989). Also, the friction coefficient increases as the coefficient of restitution decreases. The LSJC theory strongly underestimates the value of τ_{xy}/τ_{yy} for small solid fractions, but improves its prediction as v increases.

From the kinetic parts of the normal stresses, one can define 'directional' temperatures as $T_i = P_{ii}^k/n$ or, in reduced form, $\theta_i = \tau_{ii}^k/v$, which measure to what extent the granular temperature is equally distributed among the three directions of motion.
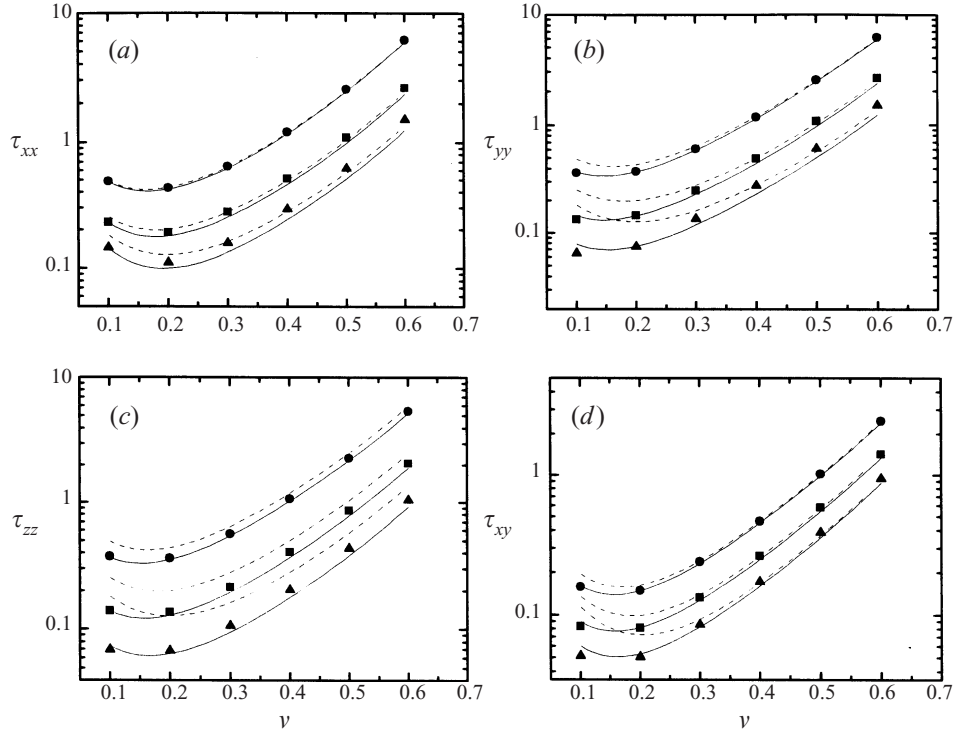
FIGURE 6. The same as in figure 5 but for the elements of the reduced stress tensor: (*a*) τ_{xx}, (*b*) τ_{yy}, (*c*) τ_{zz} and (*d*) τ_{xy}.

In figure 9 we display the ratios θ_x/θ, θ_y/θ and θ_z/θ for $\alpha = 0.6$. As v increases, the three ratios become closer to 1, thus indicating that the distribution of granular temperature becomes less anisotropic.

Apart from the rheological properties, the kinetic model provides the explicit form of the distribution function through (3.4), once T and P_{xy}^k are known. Since f depends on the three velocity components, and in order to make a comparison with the simulation results, it is convenient to consider the reduced marginal distributions $R_x(\xi_x)$ and $R_y(\xi_y)$, where

$$R_x(\xi_x) = \frac{\int_{-\infty}^{\infty} dV_y \int_{-\infty}^{\infty} dV_z\, f(V)}{\int_{-\infty}^{\infty} dV_y \int_{-\infty}^{\infty} dV_z\, f_\ell(V)} \tag{5.6}$$

and $R_y(\xi_y)$ is defined in a similar way. Here $\xi_i \equiv V_i\sqrt{m/2T}$ defines the velocity relative to the thermal velocity. The deviations of the functions $R_{x,y}$ from 1 measure the distortion of the velocity distribution from the Maxwellian. Figure 10(*a,b*) shows R_x and R_y for $\alpha = 0.8$ and $v = 0.25$. The solid lines represent the Monte Carlo data, while the dashed lines correspond to the results obtained from our kinetic model. For the sake of completeness, it is interesting to use the maximum-entropy (ME) formalism (Buck & Macaulay 1991) to construct the distribution maximizing the functional $-\int dV f(V)\ln f(V)$, subjected to the constraints of reproducing the
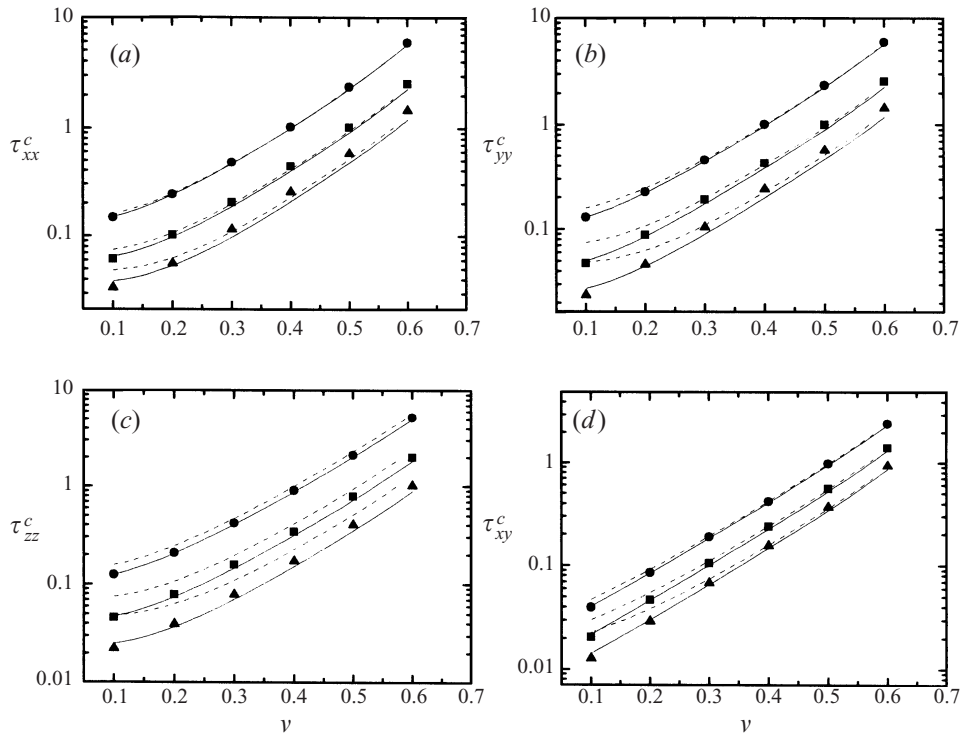
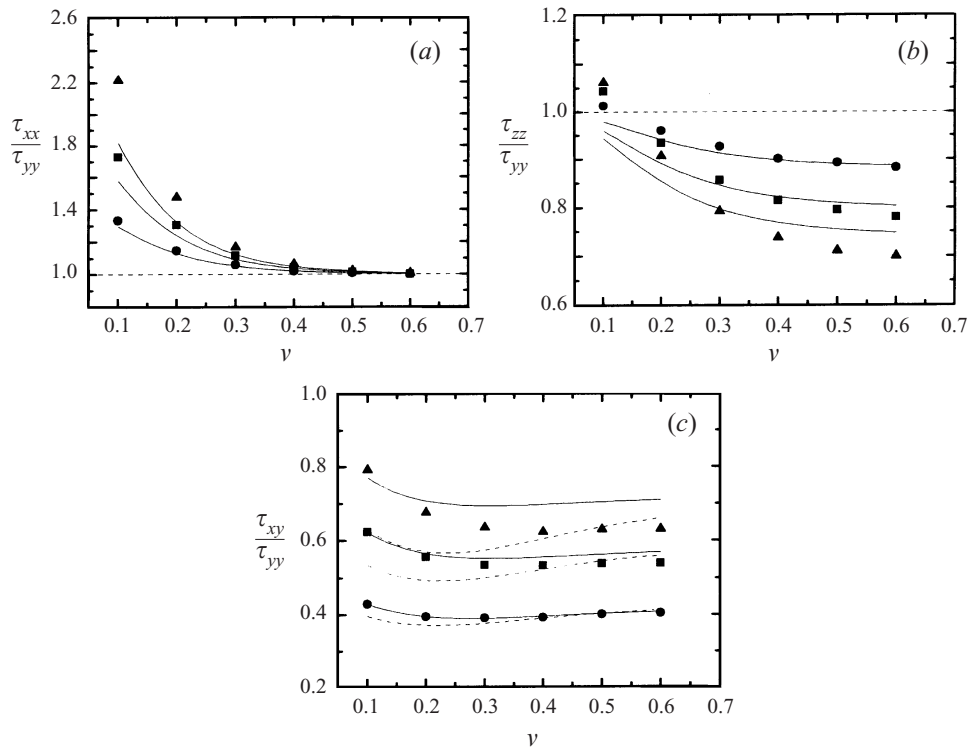FIGURE 7. The same as in figure 6 but for the collisional parts of the reduced stress tensor.

FIGURE 8. The same as in figure 5 but for the ratios (*a*) τ_{xx}/τ_{yy}, (*b*) τ_{zz}/τ_{yy} and (*c*) τ_{xy}/τ_{yy}.
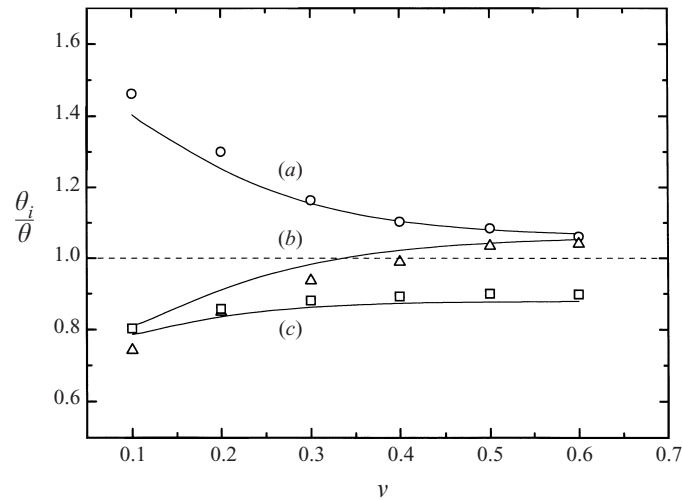
FIGURE 9. Plot of the ratios (a) θ_x/θ, (b) θ_y/θ and (c) θ_z/θ as functions of the solid fraction v for $\alpha = 0.6$. Symbols refer to simulation results and the solid lines correspond to the simplified solution of the kinetic model. The LSJC theory predicts an isotropic distribution of the granular temperature (dashed line).

density and the kinetic pressure tensor. This simply leads to

$$f(V) = n\pi^{-3/2}(\det \mathbf{Q})^{1/2}\exp(-V \cdot \mathbf{Q} \cdot V), \qquad (5.7)$$

where $\mathbf{Q} \equiv \frac{1}{2}\rho(\mathbf{P}^k)^{-1}$. The corresponding functions $R_{x,y}$ obtained from the ME approximation by using the simulation values of $\mathbf{P}^k$ are also plotted (dotted lines) in figure 10(*a,b*). The comparison shows that the ME distribution agrees better with the simulation than the kinetic model. This conclusion applies to other values of α and v as well. Notwithstanding this, it must be recalled that the kinetic model is self-consistent, while the ME method requires knowledge of the kinetic pressure tensor. The good agreement of the ME approximation found here contrasts with what happens in simple shear flows of elastic fluids (Gómez Ordóñez, Brey & Santos 1988).

Jenkins & Richman (1988) used the ME approximation (5.7) in the balance equations for $\mathbf{P}^k$ to obtain a closed set of equations (in the case of smooth hard disks). Since this set of equations is extremely difficult to solve for arbitrary values of α and v, they considered the special limits of dilute and dense systems. Even in those cases they made use of additional approximations. The fact that the ME distribution obtained from the actual values of $\mathbf{P}^k$ reproduces fairly well the simulation distribution suggests that the self-consistent solution of the Jenkins–Richman set of equations should lead to excellent values of the rheological properties. This has been confirmed by Hopkins & Shen (1992).

6. Discussion

In this paper a model kinetic equation and a Monte Carlo simulation method have been used for the study of simple shear flows of smooth inelastic hard spheres. Both approximation techniques have been developed from the Enskog equation for inelastic spheres. This implies that both approaches assume molecular chaos, i.e. the absence of correlations between pre-collisional velocities. Nevertheless, Hopkins &
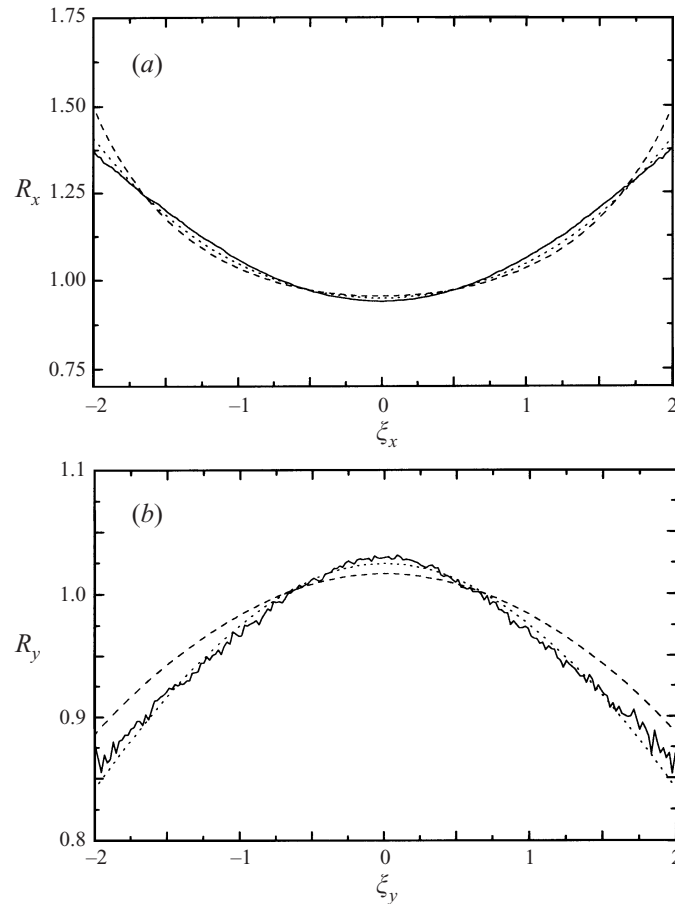
FIGURE 10. Reduced marginal distribution functions (*a*) $R_x(\xi_x)$ and (*b*) $R_y(\xi_y)$ for $\alpha = 0.8$ and $v = 0.25$. The solid lines represent the simulation results, the dashed lines are the kinetic model predictions and the dotted lines are the results obtained from the maximum-entropy approximation by using the simulation values for $\boldsymbol{P}^k$.

Shen (1992) found a remarkable agreement between Monte Carlo simulations based on the Enskog equation and Newtonian molecular dynamics, as long as the system remained as steady simple shear flow. To put the present work in a proper context, it is important to notice that we have restricted our considerations to states in which the only gradient is the one associated with the simple shear flow. Therefore, the stability of the steady state has not been investigated. In particular, density and velocity fluctuations are not allowed in the implementation of the numerical simulation. This must be taken into account when comparing the results presented here with molecular dynamics simulations, especially for small values of the coefficient of restitution. On the other hand, no restriction has been imposed on the shear rate or the inelasticity of the system. The limitations for the density range of applicability of our results are only those following from the Enskog equation, and there is no reason to expect that in the inelastic case the equation holds for a narrower interval of density than in the elastic one.

We have focused on the dependence of the (reduced) granular temperature θ and the (reduced) stress tensor τ_{ij} on the coefficient of restitution α and the solid fraction

v. The simulation results as well as the numerical solution of the kinetic model show that θ can be fitted by a linear function of $(1 - \alpha^2)^{-1}$, in agreement with molecular dynamics simulations for a dilute system (Goldhirsch & Tan 1996). In addition, τ_{xx}/θ, τ_{yy}/θ, τ_{zz}/θ and $\tau_{xy}/\theta^{1/2}$ are reasonably well represented by linear functions of $1 - \alpha^2$. The coefficients in those functions depend on *v* and have been explicitly obtained from an exact low-dissipation analysis of the kinetic model. Comparison of these simplified expressions with the simulation results shows a good quantitative agreement over a wide range of values of α and *v*. For the sake of completeness, we have also compared with the theory proposed by Lun *et al.* (1984), which is based on the Navier–Stokes solution of the Enskog equation. As expected, the agreement of this theory with simulation is good only in the case of small inelasticity. The fact that θ and τ_{ij} exhibit a relatively simple dependence on α suggests that an excellent approximation could be obtained from the solution of the Enskog equation up to super-Burnett order. This is a feasible task, although much harder than the one carried out here from a model kinetic equation.

Apart from the rheological properties, we have also obtained the velocity distribution function. While the kinetic model prediction is in good agreement with the simulation, the distribution is better described by the anisotropic Gaussian derived from the maximum-entropy (ME) method, once the simulation values of the elements of the stress tensor are known. Jenkins & Richman (1988) used the ME method to get a set of nonlinear coupled equations for those elements, but these equations are so involved that they require further approximations. It is worth pointing out that, in general, the ME approximation has been proved to give a quite poor description of far from equilibrium states of molecular systems (Gómez Ordóñez *et al.* 1988). There is no reason to expect the situation to be different for granular flows. In the absence of any other explanation we believe that the success of the ME for steady simple shear granular flow is merely accidental. Nevertheless, the theory and simulation techniques developed here can be applied in principle to any arbitrary problem, thus providing a general scheme to study rapid granular flows. In this sense, the simple shear flow problem studied in this paper illustrates that the combination of modelling and computer simulation is a very efficient way to study complex fluid states.

Appendix. Low-dissipation limit

In this Appendix we derive the expressions for the main quantities in the low-dissipation limit. In order to ease the notation, we define dimensionless quantities as follows: $V^* = (m/2T)^{1/2}V$, $f^* = n^{-1}(m/2T)^{-3/2}f$, $a^* = a/\zeta$, $P_{ij}^* = P_{ij}/nT$, $A_{ij}^* = A_{ij}/\zeta$, and $\omega^* = \omega/nT\zeta$. The objective is to expand f^*, a^*, and P_{ij}^* in powers of $\epsilon^{1/2} \equiv (1 - \alpha^2)^{1/2}$:

$$f^* = f_\ell^* + \bar{f}_1 \epsilon^{1/2} + \bar{f}_2 \epsilon + \bar{f}_3 \epsilon^{3/2} + \cdots, \tag{A 1}$$

$$a^* = \bar{a}_1 \epsilon^{1/2} + \bar{a}_3 \epsilon^{3/2} + \cdots, \tag{A 2}$$

$$P_{ij}^* = \left(1 + \tfrac{2}{3}\pi y\right) \delta_{ij} + \bar{P}_{ij,1} \epsilon^{1/2} + \bar{P}_{ij,2} \epsilon + \bar{P}_{ij,3} \epsilon^{3/2} + \cdots, \tag{A 3}$$

where $y \equiv n^* \chi = \left(\tfrac{1}{6}\pi\right)^{-1} v \chi$. For symmetry reasons, the expansion of P_{xy}^* has only odd powers, while those of the normal stresses have only even powers. From a practical

point of view, it is simpler to use a^* as a perturbation parameter instead of ϵ. This allows us to take advantage of some of the results obtained in the elastic case with a thermostat (Santos *et al.* 1998). Thus,

$$\alpha = 1 + \alpha_2 a^{*2} + \alpha_4 a^{*4} + \cdots, \tag{A 4}$$

$$f^* = f_\ell^* + f_1 a^* + f_2 a^{*2} + f_3 a^{*3} + \cdots, \tag{A 5}$$

$$\omega^* = \omega_0 + \omega_2 a^{*2} + \cdots, \tag{A 6}$$

$$P_{ij}^* = \left(1 + \tfrac{2}{3}\pi y\right)\delta_{ij} + P_{ij,1}a^* + P_{ij,2}a^{*2} + P_{ij,3}a^{*3} + \cdots, \tag{A 7}$$

$$A_{ij}^* = A_{ij,1}a^* + A_{ij,2}a^{*2} + A_{ij,3}a^{*3} + \cdots. \tag{A 8}$$

Of course, both expansions are directly related, so that

$$\bar{a}_1 = \frac{1}{(-2\alpha_2)^{1/2}}, \quad \bar{a}_3 = -\frac{1}{16\bar{a}_1\alpha_2}\left(1 + 2\frac{\alpha_4}{\alpha_2^2}\right), \tag{A 9}$$

$$\bar{f}_1 = f_1\bar{a}_1, \quad \bar{f}_2 = f_2\bar{a}_1^2, \quad \bar{f}_3 = f_3\bar{a}_1^3 + f_1\bar{a}_3. \tag{A 10}$$

The coefficients $A_{ij,\ell}$ are easily obtained from (3.5) and (3.6):

$$A_{xy,1} = -\frac{2\pi}{15}y, \quad A_{xy,3} = -\frac{2\pi}{105}y\left(14\alpha_2 + \frac{128\pi}{25}y^2\right), \quad A_{xx,2} = \frac{128\pi}{1575}y^2. \tag{A 11}$$

Let us start by obtaining the first-order coefficient f_1. Inserting the expansion (A 5) into (3.2), one gets

$$f_1(V^*) = -2\left(1 - 2A_{xy,1}\right)V_x^* V_y^* f_\ell^*(V^*). \tag{A 12}$$

From here, by velocity integration, one easily finds

$$P_{xy,1}^k = -\left(1 - 2A_{xy,1}\right) = -\left(1 + \frac{4\pi}{15}y\right). \tag{A 13}$$

Also, the collisional part can be obtained from (3.8). The result is

$$P_{xy,1}^c = -\frac{4\pi}{15}y\left(1 - 2A_{xy,1} + \frac{16}{5}y\right). \tag{A 14}$$

From the balance equation (3.1) one readily gets

$$\alpha_2 = \frac{P_{xy,1}}{2\omega_0}, \quad \omega_0 = \tfrac{5}{8}, \tag{A 15}$$

where in the last equality we have made use of (3.9).

Next, the second-order coefficient is

$$f_2(V^*) = \left[\left(1 - 2A_{xy,1}\right)\left(1 - \tfrac{2}{3}V^{*2} - 2V_y^{*2} + 4V_x^{*2}V_y^{*2}\right) + 2A_{xx,2}\left(V^{*2} - 3V_z^{*2}\right)\right]f_\ell^*(V^*). \tag{A 16}$$

Finally,

$$f_3(V^*) = 4V_x^* V_y^* \left\{\left(1 - 2A_{xy,1}\right)\left[3V_y^{*2} - 2V_x^{*2}V_y^{*2} + \tfrac{1}{3}\left(V^{*2} - \tfrac{5}{2}\right)\right]\right.$$
$$\left. + A_{xy,3} - A_{xx,2}\left(V^{*2} - 3V_z^{*2} - 1\right)\right\}f_\ell^*(V^*). \tag{A 17}$$

Equations (A 12), (A 16) and (A 17) give the explicit expression for the distribution function up to third order in a^*. Since the mathematical structure of these equations is equivalent to the one found in the elastic case by Santos *et al.* (1998), the calculation

of the corresponding contributions to the pressure tensor is similar. The results are

$$P_{xx,2}^k = \frac{4}{3}\left(1 + \frac{4\pi}{15}y + \frac{64\pi}{525}y^2\right), \tag{A 18}$$

$$P_{yy,2}^k = -\frac{2}{3}\left(1 + \frac{4\pi}{15}y - \frac{128\pi}{525}y^2\right), \tag{A 19}$$

$$P_{zz,2}^k = -\frac{2}{3}\left(1 + \frac{4\pi}{15}y + \frac{256\pi}{525}y^2\right), \tag{A 20}$$

$$P_{xy,3}^k = \frac{2}{3}\left[1 + \frac{68\pi}{75}y + \frac{128\pi}{75}\left(\frac{\pi}{5} - \frac{1}{7}\right)y^2 + \frac{256\pi^2}{1875}\left(\frac{\pi}{3} + \frac{13}{7}\right)y^3\right]. \tag{A 21}$$

$$P_{xx,2}^c = \frac{16\pi}{45}y\left[\left(1 + \frac{36}{35}y\right)\left(1 - 2A_{xy,1}\right) + \frac{144\pi}{175}y^2 + \frac{3}{2}A_{xx,2}\right] + \frac{\pi}{3}\alpha_2 y, \tag{A 22}$$

$$P_{yy,2}^c = \frac{16\pi}{45}y\left[-\left(\frac{1}{2} - \frac{36}{35}y\right)\left(1 - 2A_{xy,1}\right) + \frac{144\pi}{175}y^2 + \frac{3}{2}A_{xx,2}\right] + \frac{\pi}{3}\alpha_2 y, \tag{A 23}$$

$$P_{zz,2}^c = \frac{16\pi}{45}y\left[-\left(\frac{1}{2} - \frac{12}{35}y\right)\left(1 - 2A_{xy,1}\right) + \frac{48\pi}{175}y^2 - 3A_{xx,2}\right] + \frac{\pi}{3}\alpha_2 y, \tag{A 24}$$

$$P_{xy,3}^c = \frac{16\pi}{45}y\left\{\left[\frac{1}{2} - \frac{6}{35}A_{xy,1}y + \frac{1}{35}y\right]\left(1 - 2A_{xy,1}\right)\right.$$
$$\left. - \frac{256\pi}{875}y^3 - \frac{3}{2}A_{xx,2}\left(1 + \frac{32}{35}y\right) + \frac{3}{2}A_{xy,3}\right\} + \frac{1}{2}\alpha_2 P_{xy,1}^c. \tag{A 25}$$

Finally, knowledge of $P_{xy,3}$ allows us to get α_4 from (3.1):

$$\alpha_4 = \frac{1}{2\omega_0}\left[P_{xy,3} - \alpha_2\left(\alpha_2\omega_0 + 2\omega_2\right)\right], \tag{A 26}$$

where

$$\omega_2 = \frac{3}{32} + \frac{7\pi}{30}y + \pi\left(\frac{8}{25} + \frac{\pi}{18}\right)y^2, \tag{A 27}$$

as follows from (3.9). Inserting (A 26) into (A 9) one easily gets

$$\bar{a}_3 = \frac{\bar{a}_1^5}{2\omega_0}\left(P_{xy,3} + \frac{\omega_2}{\bar{a}_1^2}\right). \tag{A 28}$$

In summary, (A 13), (A 14) and (A 18)–(A 25) give $P_{ij,\ell}^{k,c}$, with $A_{ij,\ell}$ and α_2 given by (A 11) and (A 15), respectively. The coefficients $\bar{a}_1$ and $\bar{a}_3$ are given by (A 9), (A 27) and (A 28).

REFERENCES

BEIJEREN, H. VAN & ERNST, M. H. 1973 The modified Enskog equation. *Physica* **68**, 437–456.

BIRD, G. 1994 *Molecular Gas Dynamics and the Direct Simulation of Gas Flows.* Clarendon.

BREY, J. J. & CUBERO D. 1998 Steady state of a fluidized granular medium between two walls at the same temperature. *Phys. Rev. E* **57**, 2019–2029.

BREY, J. J., DUFTY, J. W. & SANTOS, A. 1997*a* Dissipative dynamics for hard spheres. *J. Statist. Phys.* **87**, 1051–1066.

BREY, J. J., RUIZ-MONTERO, M. J. & MORENO, F. 1997*b* Steady uniform shear flow in a low density granular gas. *Phys. Rev.* E **55**, 2846–2856.

BUCK, B. & MACAULAY, V. A. 1991 *Maximum Entropy in Action.* Clarendon.

CAMPBELL, C. S. 1989 The stress tensor for simple shear flows of a granular material. *J. Fluid Mech.* **203**, 449–473.

CAMPBELL, C. S. 1990 Rapid granular flows. *Ann. Rev. Fluid Mech.* **22**, 57–92.

CARNAHAN, N. F. & STARLING, K. E. 1969 Equation of state for nonattracting rigid spheres. *J. Chem. Phys.* **51**, 635–636.

CHAPMAN, S. & COWLING, T. G. 1970 *The Mathematical Theory of Non-Uniform Gases*, 3rd Edn. Cambridge University Press.

DUFTY, J. W., BREY, J. J. & SANTOS, A. 1997 Kinetic models for hard sphere dynamics. *Physica* A **240**, 212–220.

GOLDHIRSCH, I. & TAN, M. L. 1996 The single-particle distribution function for rapid granular shear flows of smooth inelastic disks. *Phys. Fluids* **8**, 1753–1763.

GOLDSHTEIN, A. & SHAPIRO, M. 1995 Mechanics of collisional motion of granular materials. Part 1. General hydrodynamic equations. *J. Fluid Mech.* **282**, 75–114.

GÓMEZ ORDÓÑEZ, J., BREY, J. J. & SANTOS, A. 1988 Velocity distribution of a dilute gas under uniform shear flow: Comparison between a Monte Carlo simulation method and the Bhatnagar-Gross-Krook equation. *Phys. Rev.* A **41**, 810–815.

HOPKINS, M. A. & SHEN, H. H. 1992 A Monte Carlo solution for rapidly shearing granular flows based on the kinetic theory of dense gases. *J. Fluid Mech.* **244**, 477–491.

JENKINS, J. T. & RICHMAN, M. W. 1985 Kinetic theory for plane shear flows of a dense gas of identical, rough, inelastic, circular disks. *Phys Fluids* **28**, 3485–3494.

JENKINS, J. T. & RICHMAN, M. W. 1988 Plane simple shear of smooth inelastic circular disks: the anisotropy of the second moment in the dilute and dense limits. *J. Fluid Mech.* **192**, 313–328.

JENKINS, J. T. & SAVAGE, S. B. 1983 A theory for the rapid flow of identical, smooth, nearly elastic, spherical particles. *J. Fluid Mech.* **130**, 187–202.

LUN, C. K. K. 1996 Granular dynamics of inelastic spheres in Couette flow *Phys. Fluids* **8**, 2868–2883.

LUN, C. K. K., SAVAGE, S. B., JEFFREY, D. J. & CHEPURNIY, N. 1984 Kinetic theories for granular flow: inelastic particles in Couette flow and slightly inelastic particles in a general flowfield. *J. Fluid Mech.* **140**, 223–256.

MONTANERO, J. M. & SANTOS, A. 1996 Monte Carlo simulation method for the Enskog equation. *Phys. Rev.* E **54**, 438–444.

MONTANERO, J. M. & SANTOS, A. 1997*a* Simulation of the Enskog equation *à la* Bird. *Phys. Fluids* **9**, 2057–2060.

MONTANERO, J. M. & SANTOS, A. 1997*b* Viscometric effects in a dense hard-sphere fluid. *Physica* A **240**, 229–238.

SANTOS A., MONTANERO, J. M., DUFTY J. W. & BREY, J. J. 1998 Kinetic model for the hard-sphere fluid and solid. *Phys. Rev.* E **57**, 1644–1660.

SELA N., GOLDHIRSCH, I. & NOSKOWICZ, S. H. 1996 Kinetic theoretical study of a simple sheared two-dimensional granular gas to Burnett order. *Phys. Fluids* **8**, 2337–2353.